

Superconductivity in $\text{Tl}_{0.6}\text{Bi}_2\text{Te}_3$ Derived from a Topological Insulator*

Zhiwei Wang,^{1,2} A. A. Taskin,^{1,2} Tobias Frölich,¹ Markus Braden,¹ and Yoichi Ando^{1,2,†}

¹*Institute of Physics II, University of Cologne, D-50937 Cologne, Germany*

²*Institute of Scientific and Industrial Research, Osaka University, Osaka 567-0047, Japan*

(Dated: October 7, 2018)

Bulk superconductivity has been discovered in $\text{Tl}_{0.6}\text{Bi}_2\text{Te}_3$, which is derived from the topological insulator Bi_2Te_3 . The superconducting volume fraction of up to 95% (determined from specific heat) with T_c of 2.28 K was observed. The carriers are p -type with the density of $\sim 1.8 \times 10^{20} \text{ cm}^{-3}$. Resistive transitions under magnetic fields point to an unconventional temperature dependence of the upper critical field B_{c2} . The crystal structure appears to be unchanged from Bi_2Te_3 with a shorter c lattice parameter, which, together with the Rietveld analysis, suggests that Tl ions are incorporated but not intercalated. This material is an interesting candidate of a topological superconductor which may be realized by the strong spin-orbit coupling inherent to topological insulators.

I. INTRODUCTION

The advent of topological insulators have created an exciting interdisciplinary research field which is vitalized by discoveries of new materials to realize new concepts^{1–10} and hence is greatly helped by contributions from chemistry.¹¹ The topological insulators are characterized by a gapped bulk state and gapless surface or edge states whose gapless nature is protected by time-reversal symmetry. Soon after the discovery of topological insulators, it was recognized that a similar topological state is conceivable for superconductors which also have a gapped bulk state.¹² Already various schemes for realizing such a topological superconductor (TSC) have been discussed,^{13–16} inspired by the interest in exotic quasiparticles called Majorana fermions which may show up in TSCs.¹⁷ In particular, it has been proposed¹⁸ that superconductors derived from topological insulators are promising candidates of TSCs due to the strong spin-orbit coupling which would lead to unconventional electron pairing. For superconductors of this category, a limited number of materials, such as $\text{Cu}_x\text{Bi}_2\text{Se}_3$,^{19,20} Bi_2Te_3 under high pressure,²¹ $\text{In}_x\text{Sn}_{1-x}\text{Te}$,²² $\text{Cu}_x(\text{PbSe})_5(\text{Bi}_2\text{Se}_3)_6$,²³ $\text{Sr}_x\text{Bi}_2\text{Se}_3$,²⁴ and Tl_5Te_3 ²⁵ have been discovered and studied.

Among such candidate TSCs, $\text{Cu}_x\text{Bi}_2\text{Se}_3$ was the first to show intriguing signatures of Majorana fermions on the surface.²⁶ The superconductivity in this material occurs as a result of Cu intercalation into the van der Waals gap of the parent Bi_2Se_3 compound. Although superconducting $\text{Cu}_x\text{Bi}_2\text{Se}_3$ can be grown by a melting method,¹⁹ the superconducting volume fraction (VF) is typically very low (up to $\sim 20\%$) in melt-grown samples. It was shown that an electrochemical synthesis technique²⁷ yields samples with much higher supercon-

ducting VF (up to $\sim 70\%$) near $x = 0.3$.²⁰ However, chemical differences between superconducting and non-superconducting samples of $\text{Cu}_x\text{Bi}_2\text{Se}_3$ are not understood. The superconductor phase is apparently unstable and it is easily lost by heat or mechanical strain, which makes it difficult to elucidate its exact crystal structure.

Very recently, it was found that bulk superconductivity can also be achieved in Bi_2Se_3 by intercalation of Sr; in the resulting $\text{Sr}_x\text{Bi}_2\text{Se}_3$, the maximum transition temperature T_c of 2.9 K and the superconducting VF of up to 90% have been reported.^{24,28} Also, it has been reported that all the binary topological-insulator materials having the tetradymite structure, Bi_2Se_3 , Bi_2Te_3 , and Sb_2Te_3 , become superconductors under high pressure,^{21,29,30} although it is still to be elucidated how the crystallographic and electronic structures are altered before these systems show superconductivity under pressure. Another interesting candidate of TSC is $\text{Sn}_{1-x}\text{In}_x\text{Te}$.²² This is derived from the topological crystalline insulator³¹ SnTe by doping In to the Sn site, after which the topological surface states are still preserved.³² However, the topological superconducting state appears to be limited to a narrow range of x and the condition for its realization is not clear at the moment.³³

To foster the research of TSCs, further discoveries of candidate materials are desirable. In this regard, making Bi_2Te_3 superconducting in ambient pressure by doping would be very useful, because it allows for direct comparison to $\text{Cu}_x\text{Bi}_2\text{Se}_3$ or $\text{Sr}_x\text{Bi}_2\text{Se}_3$. Like Bi_2Se_3 , pristine Bi_2Te_3 consists of covalently bonded quintuple layers (QLs) having the stacking sequence of Te-Bi-Te-Bi-Te, and those QLs are held together by van der Waals force,³⁴ which is weak enough to allow for easy exfoliation. In contrast to Bi_2Se_3 in which superconductivity is known to show up upon intercalation of Cu or Sr, no robust superconductivity has been reported for intercalated Bi_2Te_3 , besides a preliminary report³⁵ of a trace superconductivity in $\text{Pd}_x\text{Bi}_2\text{Te}_3$ which has not been confirmed by other groups. In this paper, we report that doping a large amount of Tl to Bi_2Te_3 results in a superconductor with a transition temperature of 2.28 K. A large superconducting VF of up to 95% determined from

*This document is the unedited authors' version of a submitted work that was subsequently accepted for publication in Chemistry of Materials (copyright American Chemical Society) after peer review. To access the final edited and published work see the journal's website.

specific-heat measurements gives evidence for the bulk nature of the superconductivity in $\text{Tl}_{0.6}\text{Bi}_2\text{Te}_3$. This discovery could provide a new platform for addressing topological superconductivity.

II. EXPERIMENTAL METHODS

Single crystalline samples with the nominal composition of $\text{Tl}_x\text{Bi}_2\text{Te}_3$ with various x values were synthesized from high-purity elemental shots of Tl (99.99%), Bi (99.9999%) and Te (99.9999%). We focus on samples with $x = 0.6$ in this paper, and results on other x values are presented in the Supporting Information. Before the synthesis, we performed surface cleaning procedures to remove the oxide layers formed in air on the raw shots of starting materials, as described in our previous paper.³⁶ The raw materials were then mixed with the total weight of 4.0 g and sealed in an evacuated quartz tube. The sealed quartz tubes were heated up to 1123 K and kept for 48 h with intermittent shaking to ensure homogeneity of the melt. The tubes were subsequently cooled down to 823 K at a rate of 5 K/h and, then, quenched into ice-water. We also prepared a similar sample without quenching and found that quenching is essential for obtaining superconducting samples. Large shiny single crystals with the lateral dimension of up to a few centimeters can be obtained by cleaving along the ab plane. The reference Bi_2Te_3 crystal was grown with the same method involving quenching. In addition, we also synthesized $\text{Tl}_x\text{Bi}_{2-x}\text{Te}_3$ with exactly the same method for comparison.

The crystal structure was analyzed with X-ray diffraction (XRD) using θ - 2θ scan performed on Rigaku Ultima-IV X-ray apparatus. The Rietveld analyses of powder XRD data were performed by using FullProf software package. The actual composition was analyzed by using inductively coupled plasma atomic-emission spectroscopy (ICP-AES) as well as energy-dispersive X-ray spectroscopy (EDX). DC magnetic susceptibility was measured in a SQUID magnetometer (Quantum Design MPMS). The in-plane transport properties were measured by a standard six-probe method, recording the longitudinal resistivity ρ_{xx} and the Hall resistivity ρ_{yx} simultaneously. The single crystal samples for transport measurements were cut into a rectangular shape with a typical size of $2 \times 0.5 \times 0.2 \text{ mm}^3$, and electrical contacts were made by using room-temperature-cured silver paste. The specific heat c_p was measured by a relaxation-time method using the Physical Properties Measurement System from Quantum Design equipped with a ^3He probe; the addenda signal was measured before mounting the sample and was duly subtracted from the measured signal. The c_p measurements were done in 0 T as well as in various magnetic fields up to 2 T applied along the c axis.

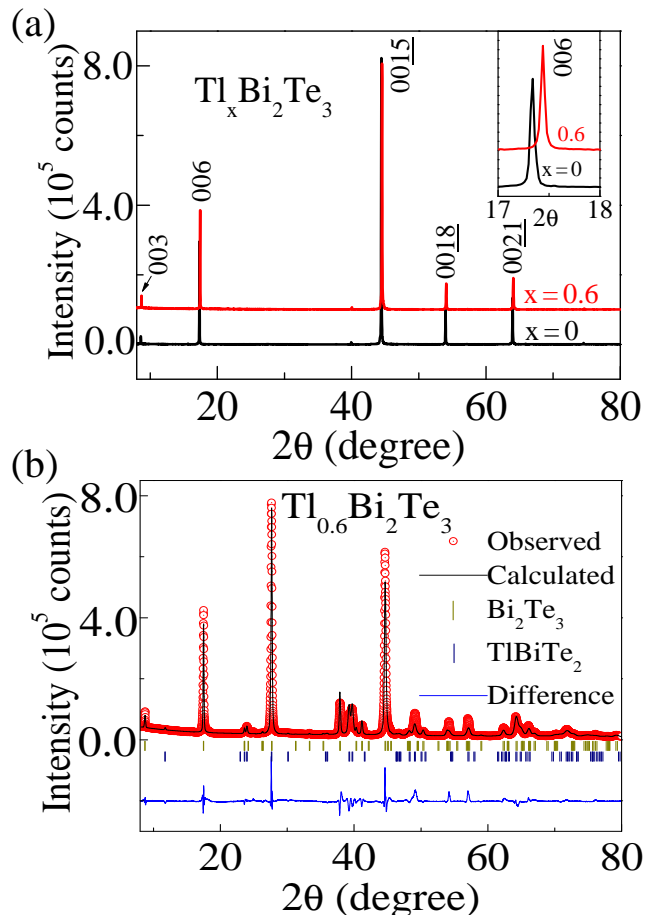


FIG. 1: (a) XRD patterns of $\text{Tl}_{0.6}\text{Bi}_2\text{Te}_3$ and Bi_2Te_3 , showing (00 l) reflections from cleaved single crystals; inset shows an enlarged view of the (006) peak, which presents a clear shift to higher angle after Tl doping. (b) Powder XRD data for $\text{Tl}_{0.6}\text{Bi}_2\text{Te}_3$ taken on powders prepared by crushing cleaved single crystals, together with the result of a Rietveld refinement to consider a coexistence of Bi_2Te_3 and TlBiTe_2 . Red symbols denote the observed intensities; black and blue lines give the calculated and difference intensities, respectively. The upper and lower lines of vertical bars indicate the positions of the Bragg reflections of the main and impurity phases, respectively.

III. RESULTS AND DISCUSSIONS

We found that quenched single crystals of $\text{Tl}_{0.6}\text{Bi}_2\text{Te}_3$ are invariably superconducting at low temperature. This composition suggests that Tl atoms are intercalated in the van der Waals gap of Bi_2Te_3 ; however, as we show in the following, the crystal structure analysis suggests that intercalation is *not* taking place. Figure 1(a) shows the XRD pattern of $\text{Tl}_{0.6}\text{Bi}_2\text{Te}_3$ measured on cleaved single crystals, along with similar data for pristine Bi_2Te_3 . The sharp reflections indicate good crystalline quality of our single crystals. Only (00 l) reflections can be observed with this method, and the peaks are easily indexed by considering the rhombohedral structure of Bi_2Te_3 .

Hence, after the doping of Tl into Bi_2Te_3 , the crystal structure remains essentially the same as that of the parent compound. However, in contrast to the cases of Cu- or Sr-doped Bi_2Se_3 , in which those dopants are intercalated into the van der Waals gap, the $(00l)$ diffraction peaks in $\text{Tl}_{0.6}\text{Bi}_2\text{Te}_3$ shift to higher 2θ angles, as one can clearly see in the inset of Figure 1(a). This means that the lattice parameter along the c -axis gets *shorter* after Tl doping. Quantitatively, it decreases from 30.606(4) Å in Bi_2Te_3 to 30.438(9) Å in $\text{Tl}_{0.6}\text{Bi}_2\text{Te}_3$. This observation suggests that intercalation is not taking place in $\text{Tl}_{0.6}\text{Bi}_2\text{Te}_3$. Note that the ICP-AES analysis indicates the existence of nearly stoichiometric amount of Tl in superconducting crystals, as shown in Table S1 of Supporting Information.

We also measured powder XRD patterns of $\text{Tl}_{0.6}\text{Bi}_2\text{Te}_3$ with Cu K_α radiation in Bragg-Brentano geometry on powders obtained from crushed crystals, and the results are shown in Figure 1(b) along with a Rietveld refinement. (Similar XRD data for smaller Tl contents are shown in Figure S1 of the Supporting Information without refinements.) We note, however, that after the grinding, the powdered samples are no longer superconducting. This suggests that the superconductor phase of $\text{Tl}_{0.6}\text{Bi}_2\text{Te}_3$ is unstable and is fragile against mechanical strain. Furthermore, we observed that the superconducting volume fraction in $\text{Tl}_{0.6}\text{Bi}_2\text{Te}_3$ diminishes with time when the samples are left at room temperature, even though they are kept in inert atmosphere or in vacuum; this suggests that doped Tl atoms are mobile even at room temperature. In passing, we have also tried to perform single-crystal XRD analysis, but $\text{Tl}_{0.6}\text{Bi}_2\text{Te}_3$ is so soft that preparations of small single crystals required for this kind of analysis resulted in deformed samples, making it impossible to obtain data of sufficient quality for the crystal structure analysis. The degradation of crystal quality was also apparent in powdered samples.

As one can see in Figure 1(b), the diffraction data are well described by two coexisting phases, Bi_2Te_3 and TlBiTe_2 , when taking the preferred orientation correction into account. The TlBiTe_2 phase possesses a volume fraction of about 35%. Attempts to refine the occupation of the Tl ions at the intercalation or other interstitial positions in the Bi_2Te_3 phase did not yield a significant occupation, in agreement with the observation that the c lattice parameter is shorter than that in pristine Bi_2Te_3 . We find a significant amount of vacancies on the Bi site (about one third), which indicates a massive occupation of the Te sites by Bi or Tl ions (i.e. Bi'_{Te} or Tl''_{Te} antisite defects). Note that Bi and Tl are indistinguishable in X-ray diffraction due to their similar atomic numbers. For the Rietveld refinement, the structure of Bi_2Te_3 with symmetry $R\bar{3}m$ (lattice constants $a = b = 4.3850(16)$ Å, $c = 30.438(9)$ Å, and $\gamma = 120^\circ$) with additional Tl positions was used. The position of the Bi-atoms was refined to $(0, 0, 0.3988(3))$ at the Wyckoff position 6c, the positions of the Te-atoms were $(0, 0, 0)$ at the Wyckoff

position 3a and $(0, 0, 0.8043(2))$ at the Wyckoff position 6c. No significant occupation of additional Tl-atoms at $(0.5, 0, 0.5)$ or $(0.0, 0, 0.5)$ could be determined. All positions refer to the hexagonal setting of the rhombohedral cell. The TlBiTe_2 impurity phase was also described in space group $R\bar{3}m$ (lattice constants $a = b = 4.539(1)$ Å, $c = 22.617(8)$ Å, and $\gamma = 120^\circ$) and only the z position of the Te site was refined to $(0, 0, 0.2446(10))$.

Although TlBiTe_2 was reported to become superconducting below 0.14 K,³⁷ this impurity phase cannot be responsible for the appearance of the superconductivity in our samples, whose T_c is above 2 K. It is also worth mentioning that elemental thallium metal is superconducting with T_c of ~ 2.4 K,³⁸ which is close to the T_c of $\text{Tl}_{0.6}\text{Bi}_2\text{Te}_3$. However, it is very unlikely that the superconductivity observed here is due to elemental thallium, because the XRD data do not indicate the existence of thallium metal in our samples.

In the past, the crystal structure of Tl-doped Bi_2Te_3 with the composition of $\text{Tl}_x\text{Bi}_{2-x}\text{Te}_3$ was studied.^{39,40} It was concluded that, even though the composition suggests that Tl atoms partially substitute the Bi sites of the Bi_2Te_3 lattice, what actually happens is that Tl nucleates microscopic patches of nominal $\text{Te-Bi-Te-Tl-V}_{\text{Te}}^{\bullet\bullet}$ layer, which is derived from TlBiTe_2 structure and has the same symmetry as the Bi_2Te_3 phase^{39,40} (in real crystals, the fictitious plane of Te vacancy would be partially filled with Te, distributing $V_{\text{Te}}^{\bullet\bullet}$ to the neighboring Te plane of Bi_2Te_3). It was proposed that there are random microscopic formations of this defect layer in Tl-doped Bi_2Te_3 , which results in the overall crystal structure to be the same as Bi_2Te_3 and causes little change in the lattice constants, even though a significant amount of Tl is incorporated into the lattice.

It is useful to note that both our ICP-AES and EDX analyses of the crystals indicate the presence of nearly stoichiometric amount of Tl, which would give rise to about 30% of the TlBiTe_2 phase if the sample phase-separates into Bi_2Te_3 and TlBiTe_2 . The amount of the TlBiTe_2 phase indicated in the Rietveld refinement is consistent with this estimate, which suggests that due to the mobility of Tl atoms at room temperature, the material actually phase separates into Bi_2Te_3 and TlBiTe_2 upon grinding. This in turn suggests that it is very difficult to elucidate the crystal structure of the superconductor phase.

A possible picture, which one can speculate for the superconducting phase based on the above result, would be to consider the formation of the nominal $\text{Te-Bi-Te-Tl-V}_{\text{Te}}^{\bullet\bullet}$ defect layer in the Bi_2Te_3 lattice, as is the case of the $\text{Tl}_x\text{Bi}_{2-x}\text{Te}_3$ compound.^{39,40} This defect layer may eventually cluster to form the TlBiTe_2 phase. An important difference from the case of the $\text{Tl}_x\text{Bi}_{2-x}\text{Te}_3$ compound would be that a sizable portion of Bi atoms in $\text{Tl}_{0.6}\text{Bi}_2\text{Te}_3$ are most likely partially filling the Te sites of the Bi_2Te_3 lattice and form Bi'_{Te} antisite defects, which is consistent with the result of the Rietveld refinement. In fact, the composition of $\text{Tl}_{0.6}\text{Bi}_2\text{Te}_3$ would create a sig-

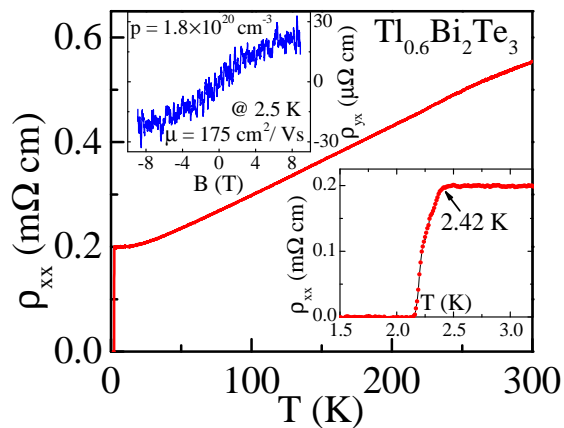


FIG. 2: Temperature dependence of the in-plane resistivity ρ_{xx} in $\text{Tl}_{0.6}\text{Bi}_2\text{Te}_3$. Upper inset shows the magnetic-field dependence of the Hall resistivity ρ_{yx} of the same sample at 2.5 K; lower inset shows the $\rho_{xx}(T)$ behavior near the transition.

nificantly Te-deficient growth condition and promote the formation of Bi'_{Te} antisite defects.⁴¹ In any case, the precise structure of superconducting $\text{Tl}_{0.6}\text{Bi}_2\text{Te}_3$ should be determined in future studies, possibly by neutron scattering on as-grown crystals.

Figure 2 shows the temperature dependence of ρ_{xx} in $\text{Tl}_{0.6}\text{Bi}_2\text{Te}_3$ at zero field. The onset of superconducting transition occurs at $T \approx 2.42$ K, and the zero resistivity is achieved at $T \approx 2.15$ K (lower inset of Figure 2), indicating a relatively sharp transition. The resistivity in the normal state shows a metallic behavior with the residual resistivity $\rho_0 = 2 \times 10^{-4}$ Ωcm . The magnetic-field dependence of ρ_{yx} at 2.5 K is shown in the upper inset of Figure 2; this $\rho_{yx}(B)$ behavior is slightly non-linear, which suggests the existence of two or more bands at the Fermi level. Also, the $\rho_{yx}(B)$ data indicate that the main carriers are p -type (i.e. holes), and from the slope near 0 T we calculate the approximate carrier density of $p \approx 1.8 \times 10^{20}$ cm^{-3} . From p and ρ_0 , one obtains the mobility $\mu \approx 175$ cm^2/Vs . It is important to note that the carrier type is different from the case of Cu- or Sr-intercalated Bi_2Se_3 superconductors, in which the carriers are n -type.^{19,20,24} Nevertheless, the magnitude of the carrier density, about 2×10^{20} cm^{-3} , is comparable to that in $\text{Cu}_x\text{Bi}_2\text{Se}_3$.^{19,20} Hence, $\text{Tl}_{0.6}\text{Bi}_2\text{Te}_3$ would allow for investigation of the roles of the carrier types in producing a topological superconducting state in otherwise similar settings, if this material turns out to be a TSC. In passing, we comment on the possible impact of the TlBiTe_2 impurity phase and the nominal $\text{Te-Bi-Te-Tl-V}_{\text{Te}}^{\bullet\bullet}$ defect layer on the transport properties. While the direct impact of phase-separated TlBiTe_2 impurity phase is expected to be minor because the carrier density of this phase is similar to that of the main phase,³⁷ the defect layer may be working as strong scatters of charge carriers and is possibly playing some role in the occurrence of superconductivity.

Figure 3(a) shows the temperature dependence of the

shielding fraction in $\text{Tl}_{0.6}\text{Bi}_2\text{Te}_3$ measured under 0.2 mT applied parallel to the ab -plane to minimize the demagnetization effect; the configuration is schematically shown in the inset. Note that the shielding fraction is defined as the fraction of the sample volume from which the magnetic field is kept out due to superconductivity; the data for both field-cooled (FC) and zero-field-cooled (ZFC) measurements are shown. The onset of superconducting transition is observed at $T \simeq 2.35$ K. This is consistent with the resistivity transition shown in Figure 2. Furthermore, the ZFC shielding fraction at 1.75 K is as much as 83%, pointing to bulk superconductivity.

We have also synthesized $\text{Tl}_x\text{Bi}_2\text{Te}_3$ samples with various x values, and it was found that both T_c and the shielding fraction become lower for $x < 0.6$, as is shown in Figure S2 of the Supporting Information. Also, for $x > 0.6$, we found that the TlBiTe_2 impurity phase becomes dominant and it was impossible to synthesize large single crystals retaining the Bi_2Te_3 structure. Therefore, we concluded that $x = 0.6$ is the optimum composition for this new superconductor.

The magnetization curve $M(B)$ measured at 1.75 K with the magnetic field applied parallel to the ab plane is shown in Figure 3(b). This $M(B)$ behavior indicates that $\text{Tl}_{0.6}\text{Bi}_2\text{Te}_3$ is a type-II superconductor and the flux pinning is very weak, as was also the case in $\text{Cu}_x\text{Bi}_2\text{Se}_3$.²⁰ From the low-field $M(B)$ behavior measured after zero-field cooling (shown in Figure S3 of Supporting Information), one can determine the lower critical field B_{c1} as the characteristic field above which the $M(B)$ data start to deviate from the initial linear behavior; at the lowest temperature of 1.75 K, B_{c1} is estimated to be 0.35 mT, which is very small and is comparable to that in $\text{Cu}_x\text{Bi}_2\text{Se}_3$.^{19,20} Such a low B_{c1} value means a very low superfluid density, which is consistent with the low carrier density.

Figure 4 shows the plots of c_p/T vs T measured in 0 T and 2 T applied perpendicular to the ab -plane, as schematically shown in the inset; since the superconductivity is completely suppressed in 2 T as we show later, the 2-T data represent the normal-state behavior. A fitting of the normal-state data to the conventional Debye formula $c_p = \gamma_n T + A_3 T^3 + A_5 T^5$, shown as the dashed line in Figure 4(a), gives the following parameters: $\gamma_n = 4.8$ mJ/mol-K^2 , $A_3 = 4.4$ mJ/mol-K^4 , and $A_5 = 0.11$ mJ/mol-K^6 . The electronic specific heat c_{el}/T in the SC state is obtained by subtracting the phononic contribution $A_3 T^3 + A_5 T^5$ from the zero-field data, and the result is plotted in Figure 4(b). The pronounced jump gives evidence for the bulk nature of the superconductivity in $\text{Tl}_{0.6}\text{Bi}_2\text{Te}_3$, and this anomaly provides an accurate measure of $T_c = 2.28$ K. Fitting of $c_{el}(T)/T$ to the BCS model⁴² reproduces the zero-field data very well if one assumes a 95% superconducting VF. Therefore, one may conclude that the superconducting state of $\text{Tl}_{0.6}\text{Bi}_2\text{Te}_3$ is fully gapped. Note that the applicability of the BCS model to the specific-heat data does not exclude the possibility of unconventional odd-parity

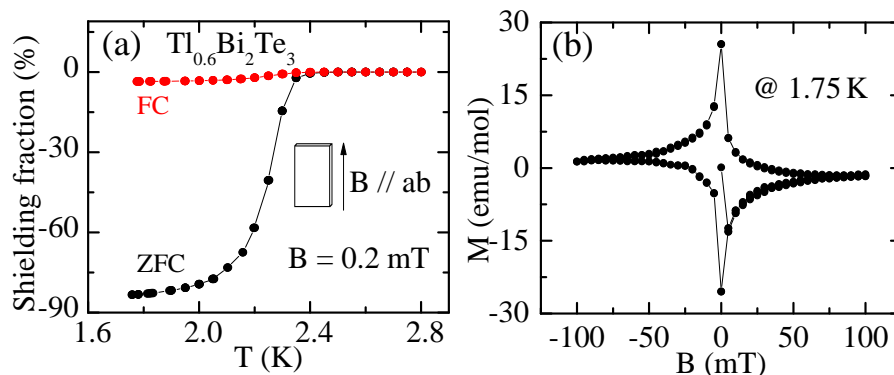


FIG. 3: (a) Temperature dependence of the magnetic susceptibility in $\text{Tl}_{0.6}\text{Bi}_2\text{Te}_3$ under 0.2 mT for FC and ZFC measurements, plotted in terms of the shielding fraction. (b) Plot of magnetization M vs magnetic field B at 1.75 K.

pairing.²⁰ The superconducting VF of 95% is incompatible with the 35% inclusion of TlBiTe_2 phase suggested by the Rietveld analysis on crushed crystals, and this incompatibility supports our speculation that a sizable amount of TlBiTe_2 phase is created upon grinding.

To determine the upper critical field B_{c2} , the magnetic-field dependences of ρ_{xx} at various temperatures down to 0.42 K were measured in fields perpendicular to the ab -plane [Figure 5(a)]. For the analysis of the resistive transitions, both the 50% and 90% levels of the normal-state resistivity ρ_N (shown by dashed lines) are taken as characteristic levels to mark the transition; the difference between these two criteria gives an idea about the uncertainty in determining B_{c2} from resistive transitions. In addition, the $c_{el}(T)/T$ behavior was measured in various magnetic-field strengths [Figure 5(b)], and we take

the mid-point of the specific-heat jump as the definition of the thermodynamic transition. Note that the data shown in Figures 2 – 5 are all taken on the same sample. The summary of B_{c2} thus determined are plotted in Figure 5(c). The Werthamer-Helfand-Hohenberg (WHH) theory⁴³ fits the thermodynamic $B_{c2}(T)$ obtained from specific heat very well and gives $B_{c2}(0)$ of 1.06 T, which corresponds to the coherence length $\xi = \sqrt{\Phi_0/(2\pi B_{c2})} = 17.6$ nm. On the other hand, the $B_{c2}(T)$ extracted from resistive transitions do not follow the WHH behavior and extrapolates to a higher $B_{c2}(0)$; such a behavior has been reported for $\text{Cu}_x\text{Bi}_2\text{Se}_3$ and also for pressurized Bi_2Se_3 , and was argued as evidence for unconventional superconductivity.^{29,44}

IV. CONCLUSIONS

The discovery of superconductivity in $\text{Tl}_{0.6}\text{Bi}_2\text{Te}_3$ widens the opportunities to elucidate topological superconductivity in topological-insulator-based superconductors, particularly since the superconducting VF of up to 95% is achievable. Various aspects of the superconductivity in $\text{Tl}_{0.6}\text{Bi}_2\text{Te}_3$, including the unconventional resistive $B_{c2}(T)$ behavior and the very small B_{c1} value, are similar to those found in $\text{Cu}_x\text{Bi}_2\text{Se}_3$. Nevertheless, the carrier type is opposite, which may prove useful for understanding the mechanism of superconductivity. The crystal structure of this material appears to be essentially unchanged from that of Bi_2Te_3 with a slightly shorter c -axis length and no interstitials, but it turned out to be difficult to elucidate the exact structure of the superconductor phase.

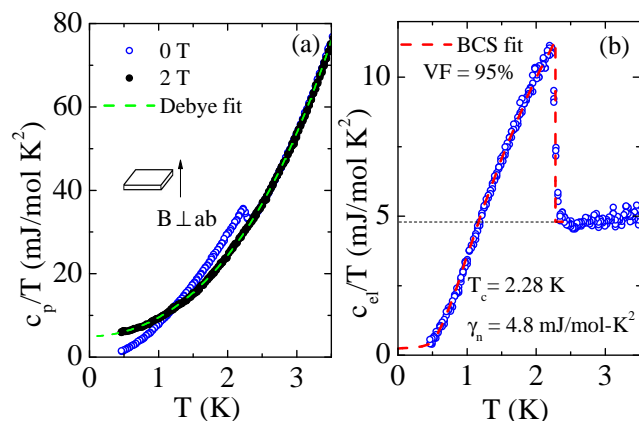


FIG. 4: (a) Plots of $c_p(T)/T$ vs T for $\text{Tl}_{0.6}\text{Bi}_2\text{Te}_3$ measured in 0 and 2 T applied along the c axis; dashed line shows the conventional Debye fitting. (b) The electronic contribution c_{el}/T in 0 T obtained after subtracting the phonon term determined in 2 T; dashed line shows a BCS-model fitting assuming 95% superconducting volume fraction.

V. SUPPORTING INFORMATION

Table showing the results of ICP-AES analysis; powder XRD data for smaller Tl contents; superconducting transitions in crystals with smaller Tl contents probed

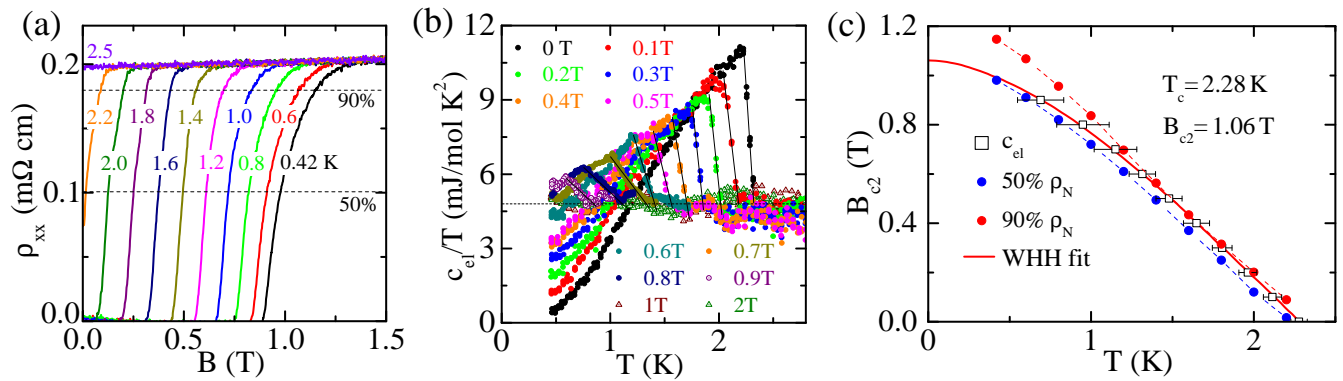


FIG. 5: (a) $\rho_{xx}(B)$ curves for $\text{Tl}_{0.6}\text{Bi}_2\text{Te}_3$ in the transition region at various temperatures. The magnetic-field direction is perpendicular to the ab plane. (b) Plots of $c_{el}(T)/T$ vs T in various magnitudes of perpendicular magnetic field. (c) B_{c2} vs T phase diagram determined from 50% ρ_N (red circles), 90% ρ_N (blue circles), and c_{el} (black squares) data; the error bar on the data points from c_{el} corresponds to the width of the specific-heat jump. The solid line shows the WHH fitting to the thermodynamic $B_{c2}(T)$ obtained from c_{el} .

by magnetic susceptibility; virgin $M(B)$ curve for determining B_{c1} .

VI. ACKNOWLEDGMENT

This work was supported by Japan Society for the Promotion of Science (KAKENHI 25220708 and 25400328)

and the Excellence Initiative of the German Research Foundation.

- [†] Electronic address: ando@ph2.uni-koeln.de
- ¹ König, M.; Wiedmann, S.; Brüne, C.; Roth, A.; Buhmann, H.; Molenkamp, L.W.; Qi, X.-L.; Zhang, S.-C. Quantum Spin Hall Insulator State in HgTe Quantum Wells. *Science* **2007**, 318, 766-770.
 - ² Fu, L.; Kane, C. L.; Mele, E. J. Topological Insulators in Three Dimensions. *Phys. Rev. Lett.* **2007**, 98, 106803.
 - ³ Moore, J. E.; Balents, L. Topological Invariants of Time-reversal-invariant Band Structures. *Phys. Rev. B* **2007**, 75, 121306(R).
 - ⁴ Hsieh, D.; Qian, D.; Wray, L.; Xia, Y.; Hor, Y. S.; Cava, R. J.; Hasan, M. Z. A Topological Dirac Insulator in a Quantum Spin Hall Phase. *Nature* **2008**, 452, 970-974.
 - ⁵ Roy, R. Topological Phases and the Quantum Spin Hall Effect in Three Dimensions. *Phys. Rev. B* **2009**, 79, 195332.
 - ⁶ Taskin, A. A.; Ando, Y. Quantum Oscillations in a Topological Insulator $\text{Bi}_{1-x}\text{Sb}_x$. *Phys. Rev. B* **2009**, 80, 085303.
 - ⁷ Sato, T.; Segawa, K.; Guo, H.; Sugawara, K.; Souma, S.; Takahashi, T.; Ando, Y. Direct Evidence for the Dirac-Cone Topological Surface States in the Ternary Chalcogenide TlBiSe_2 . *Phys. Rev. Lett.* **2010**, 105, 136802.
 - ⁸ Hasan, M.Z.; Kane, C.L. Colloquium: Topological Insulators. *Rev. Mod. Phys.* **2010**, 82, 3045-3067.
 - ⁹ Qi, X.-L.; Zhang, S.-C. Topological Insulators and Superconductors. *Rev. Mod. Phys.* **2011**, 83, 1057-1110.
 - ¹⁰ Ando, Y. Topological Insulator Materials. *J. Phys. Soc. Jpn.* **2013**, 82, 102001.
 - ¹¹ Cava, R. J.; Ji, H.; Fuccillo, M. K.; Gibson, Q. D.; Hor, Y. S. Crystal Structure and Chemistry of Topological Insulators. *J. Mater. Chem. C* **2013**, 1, 3176-3189.
 - ¹² Schnyder, A. P.; Ryu, S.; Furusaki, A.; Ludwig, A. W. W. Classification of Topological Insulators and Superconductors in Three Spatial Dimensions. *Phys. Rev. B* **2008**, 78, 195125.
 - ¹³ Fu, L.; Kane, C. L. Superconducting Proximity Effect and Majorana Fermions at the Surface of a Topological Insulator. *Phys. Rev. Lett.* **2008**, 100, 096407.
 - ¹⁴ Qi, X.-L.; Hughes, T. L.; Raghu, S.; Zhang, S.-C. Time-Reversal-Invariant Topological Superconductors and Superfluids in Two and Three Dimensions. *Phys. Rev. Lett.* **2009**, 102, 187001.
 - ¹⁵ Sato, M. Topological Odd-parity Superconductors. *Phys. Rev. B* **2010**, 81, 220504(R).
 - ¹⁶ Linder, J.; Tanaka, Y.; Yokoyama, T.; Sudbø, A.; Nagaosa, N. Unconventional Superconductivity on a Topological Insulator. *Phys. Rev. Lett.* **2010**, 104, 067001.
 - ¹⁷ Wilczek, F. Majorana Returns. *Nature Physics* **2009**, 5, 614-618.
 - ¹⁸ Fu, L.; Berg, E., Odd-Parity Topological Superconductors: Theory and Application to $\text{Cu}_x\text{Bi}_2\text{Se}_3$. *Phys. Rev. Lett.* **2010**, 105, 097001.
 - ¹⁹ Hor, Y. S.; Williams, A. J.; Checkelsky, J. G.; Roushan, P.; Seo, J.; Xu, Q.; Zandbergen, H. W.; Yazdani, A.; Ong, N. P.; Cava, R. J. Superconductivity in $\text{Cu}_x\text{Bi}_2\text{Se}_3$ and its Implications for Pairing in the Undoped Topological Insulator. *Phys. Rev. Lett.* **2010**, 104, 057001.

- ²⁰ Kriener, M.; Segawa, K.; Ren, Z.; Sasaki, S.; Ando, Y. Bulk Superconducting Phase with a Full Energy Gap in the Doped Topological Insulator $\text{Cu}_x\text{Bi}_2\text{Se}_3$. *Phys. Rev. Lett* **2011**, 106, 127004.
- ²¹ Zhang, J. L.; Zhang, S. J.; Weng, H. M.; Zhang, W.; Yang, L. X.; Liu, Q. Q.; Feng, S. M.; Wang, X. C.; Yu, R. C.; Cao, L. Z.; Wang, L.; Yang, W. G.; Liu, H. Z.; Zhao, W. Y.; Zhang, S. C.; Dai, X.; Fang, Z.; Jin, C. Q. Pressure-induced Superconductivity in Topological Parent Compound Bi_2Te_3 . *Proc. Natl. Acad. Sci.* **2011**, 108, 24.
- ²² Sasaki, S.; Ren, Z.; Taskin, A. A.; Segawa, K.; Fu, L.; Ando, Y. Odd-Parity Pairing and Topological Superconductivity in a Strongly Spin-Orbit Coupled Semiconductor. *Phys. Rev. Lett* **2012**, 109, 217004.
- ²³ Sasaki, S.; Segawa, K.; Ando, Y. Superconductor Derived from a Topological Insulator Heterostructure. *Phys. Rev. B* **2014**, 90, 220504.
- ²⁴ Liu, Z.; Yao, X.; Shao, J.; Zuo, M.; Pi, L.; Tan, S.; Zhang, C.; Zhang, Y. Superconductivity with Topological Surface State in $\text{Sr}_x\text{Bi}_2\text{Se}_3$. *J. Am. Chem. Soc.* **2015**, 137, 10512-10515.
- ²⁵ Arpino, K. E.; Wallace, D. C.; Nie, Y. F.; Birol, T.; King, P. D. C.; Chatterjee, S.; Uchida, M.; Koohpayeh, S. M.; Wen, J. J.; Page, K.; Fennie, C. J.; Shen, K. M.; McQueen, T. M. Evidence for Topologically Protected Surface States and a Superconducting Phase in $[\text{Ti}_4](\text{Ti}_{0.4}\text{Sn}_{0.6})\text{Te}_3$ Using Photoemission, Specific Heat, and Magnetization Measurements, and Density Functional Theory. *Phys. Rev. Lett.* **2014**, 112, 017002.
- ²⁶ Sasaki, S.; Kriener, M.; Segawa, K.; Yada, K.; Tanaka, Y.; Sato, M.; Ando, Y. Topological Superconductivity in $\text{Cu}_x\text{Bi}_2\text{Se}_3$. *Phys. Rev. Lett* **2011**, 107, 217001.
- ²⁷ Kriener, M.; Segawa, K.; Ren, Z.; Sasaki, S.; Wada, S.; Kuwabata, S.; Ando, Y. Electrochemical Synthesis and Superconducting Phase Diagram of $\text{Cu}_x\text{Bi}_2\text{Se}_3$. *Phys. Rev. B* **2011**, 84, 054513.
- ²⁸ Shruti; Maurya, V. K.; Neha, P.; Srivastava, P.; Patnaik, S. Superconductivity by Sr Intercalation in Layered Topological Insulator Bi_2Se_3 . **2015**, arXiv:1505.05394.
- ²⁹ Kirshenbaum, K.; Syers, P. S.; Hope, A. P.; Butch, N. P.; Jeffries, J. R.; Weir, S. T.; Hamlin, J. J.; Maple, M. B.; Vohra, Y. K.; Paglione, J. Pressure-Induced Unconventional Superconducting Phase in the Topological Insulator Bi_2Se_3 . *Phys. Rev. Lett* **2013**, 111, 087001.
- ³⁰ Zhu, J.; Zhang, J. L.; Kong, P. P.; Zhang, S. J.; Yu, X. H.; Zhu, J. L.; Liu, Q. Q.; Li, X.; Yu, R. C.; Ahuja, R.; Yang, W. G.; Shen, G. Y.; Mao, H. K.; Weng, H. M.; Dai, X.; Fang, Z.; Zhao, Y. S.; Jin, C. Q. Superconductivity in Topological Insulator Sb_2Te_3 Induced by Pressure. *Sci. Rep.* **2013**, 3, 02016.
- ³¹ Ando, Y.; Fu, L., Topological Crystalline Insulators and Topological Superconductors: From Concepts to Materials. *Annual Review of Condensed Matter Physics* **2015**, 6, 361-381.
- ³² Sato, T.; Tanaka, Y.; Nakayama, K.; Souma, S.; Takahashi, T.; Sasaki, S.; Ren, Z.; Taskin, A. A.; Segawa, K.; Ando, Y. Fermiology of the Strongly Spin-Orbit Coupled Superconductor $\text{Sn}_{1-x}\text{In}_x\text{Te}$: Implications for Topological Superconductivity. *Phys. Rev. Lett* **2013**, 110, 206804.
- ³³ Novak, M.; Sasaki, S.; Kriener, M.; Segawa, K.; Ando, Y. Unusual Nature of Fully Gapped Superconductivity in In-doped SnTe . *Phys. Rev. B* **2013**, 88, 140502(R).
- ³⁴ Wiese, J. R.; Muldrew, L. Lattice Constants of Bi_2Te_3 - Bi_2Se_3 Solid Solution Alloys. *J. Phys. Chem. Solids* **1960**, 15, 13-16.
- ³⁵ Hor, Y. S.; Checkelsky, J. G.; Qu, D.; Ong, N. P.; Cava, R. J. Superconductivity and Non-metallicity Induced by Doping the Topological Insulators Bi_2Se_3 and Bi_2Te_3 . *J. Phys. Chem. Solids* **2011**, 72, 572-576.
- ³⁶ Wang, Z.; Segawa, K.; Sasaki, S.; Taskin, A. A.; Ando, Y. Ferromagnetism in Cr-doped Topological Insulator TlSbTe_2 . *APL Materials* **2015**, 3, 083302.
- ³⁷ Hein, R. A.; Swiggard, E. M. Superconductivity in TlBiTe_2 : A Low Carrier Density (III-V)VI₂ Compound. *Phys. Rev. Lett* **1970**, 24, 53-55.
- ³⁸ Eisenstein, J., Superconducting Elements. *Rev. Mod. Phys.* **1954**, 26, 277-291.
- ³⁹ Lostak, P.; Bezdzicka, P.; Horak, J.; Sramkova, J., Electrical and optical properties of TL-doped Bi_2Te_3 crystals. *Radiat Eff. Defects Solids* **2006**, 138, 251-260.
- ⁴⁰ Chi, H.; Liu, W.; Sun, K.; Su, X.; Wang, G.; Lostak, P.; Kucek, V.; Drasar, C.; Uher, C., Low-temperature transport properties of TI-doped Bi_2Te_3 single crystals. *Phys. Rev. B* **2013**, 88, 045202.
- ⁴¹ Scanlon, D. O.; King, P. D. C.; Singh, R. P.; de la Torre, A.; Walker, S. M.; Balakrishnan, G.; Baumberger, F.; Catlow, C. R. A., Controlling Bulk Conductivity in Topological Insulators: Key Role of Anti-Site Defects. *Adv. Mater.* **2012**, 24, 2154-2158.
- ⁴² Tinkham, M. Introduction to Superconductivity (McGraw-Hill, New York, 1975).
- ⁴³ Werthamer, N. R.; Helfand, K.; Hohenberg, P. C. Temperature and Purity Dependence of the Superconducting Critical Field, H_{c2} . III. Electron Spin and Spin-Orbit Effects. *Phys. Rev.* **1966**, 147, 295-302.
- ⁴⁴ Bay, T. V.; Naka, T.; Huang, Y. K.; Luigjes, H.; Golden, M. S.; de Visser, A. Superconductivity in the Doped Topological Insulator $\text{Cu}_x\text{Bi}_2\text{Se}_3$ under High Pressure. *Phys. Rev. Lett.* **2012**, 108, 057001.

Supporting Information

x	Nominal composition	Tl	Bi	Te
0.1	Tl _{0.1} Bi ₂ Te ₃	0.106(1)	2.087(6)	3
0.2	Tl _{0.2} Bi ₂ Te ₃	0.207(2)	2.098(6)	3
0.3	Tl _{0.3} Bi ₂ Te ₃	0.233(2)	2.090(6)	3
0.4	Tl _{0.4} Bi ₂ Te ₃	0.396(4)	2.077(6)	3
0.5	Tl _{0.5} Bi ₂ Te ₃	0.526(5)	2.040(6)	3
0.6	Tl _{0.6} Bi ₂ Te ₃	0.609(6)	2.059(6)	3

TABLE I: Molar ratio of Tl, Bi, and Te in the single-crystal samples of Tl _{x} Bi₂Te₃. The data are obtained from ICP-AES analyses. The tellurium composition is fixed to be 3.

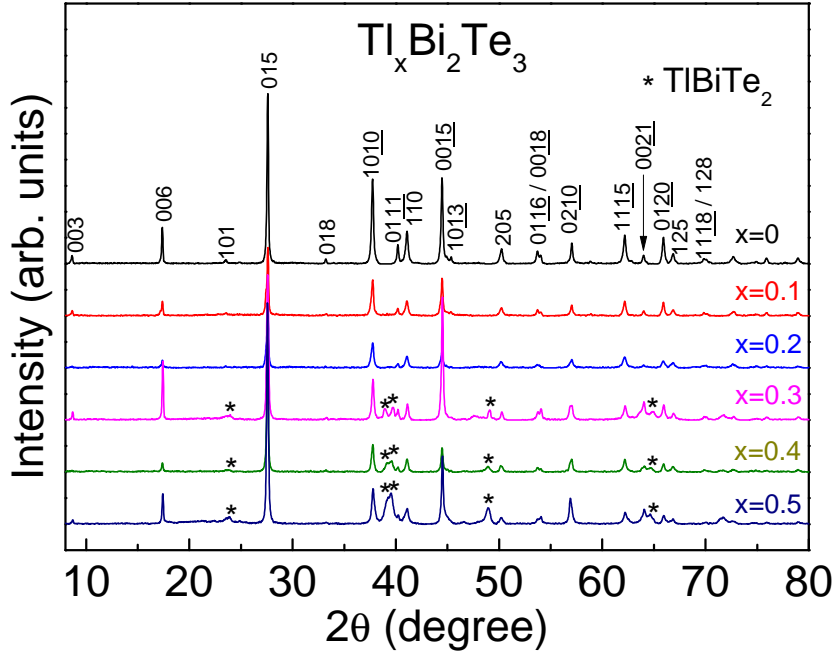


FIG. S1: Powder XRD patterns of Tl _{x} Bi₂Te₃ ($x = 0.1, 0.2, 0.3, 0.4,$ and 0.5) and Bi₂Te₃, taken on powders prepared by crushing cleaved single crystals. The peaks due to the TlBiTe₂ impurity phase are indicated with asterisks, and they are discernible in the data for $x = 0.3, 0.4,$ and 0.5 .

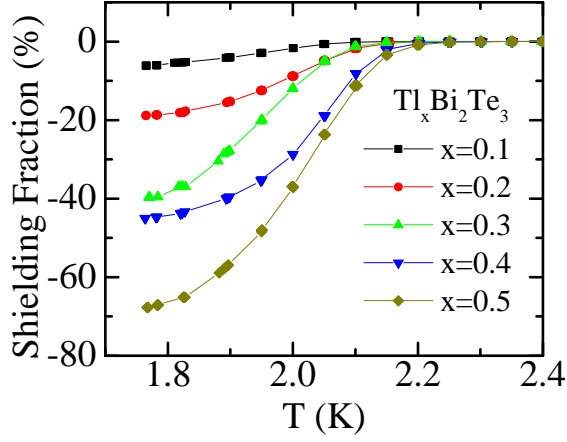


FIG. S2: Temperature dependence of the magnetic susceptibility in $\text{Tl}_x\text{Bi}_2\text{Te}_3$ with $x = 0.1 - 0.5$ measured under 0.2 mT, plotted in terms of the shielding fraction.

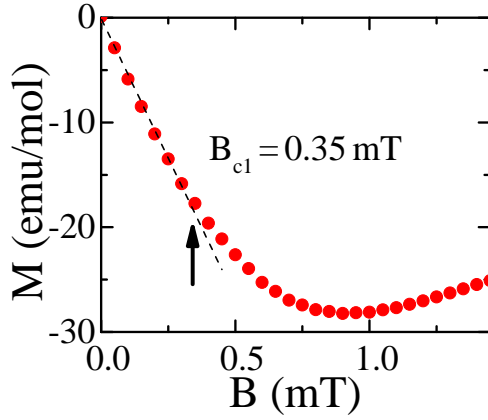


FIG. S3: Virgin $M(B)$ curve of $\text{Tl}_{0.6}\text{Bi}_2\text{Te}_3$ at 1.75 K measured after zero-field cooling the sample. The magnetic field was applied parallel to the ab plane to minimize the demagnetization effect.